Hindawi
International Journal of Antennas and Propagation
Volume 2023, Article ID 5664588, 12 pages
https://doi.org/10.1155/2023/5664588

Research Article

An Ultrathin Polarization Free Asterick-Shaped Metamaterial Absorber with Quad-Band Characteristics

Raghvenda Kumar Singh, Ashish Gupta, Akash Yadav, Nishchay Gupta, and Utkarsh Tyagi

Department of Electronics and Communication Engineering, Jaypee Institute of Information Technology, Noida 201304, Uttar Pradesh, India

Correspondence should be addressed to Ashish Gupta; ashish.gupta@jiit.ac.in

Received 20 May 2023; Revised 25 June 2023; Accepted 18 August 2023; Published 5 September 2023

Academic Editor: Miguel Ferrando Bataller

In this paper, a quad-band absorber is proposed and developed, which is exhibiting ultrathin and polarization insensitive behaviour. It has been designed to be operated in S, C, and Ku bands with absorptions peaks at more than 95%. The proposed absorber is implemented on a FR4 glass epoxy laminate with an equivalent electrical thickness of 0.0108 λ_0, where λ_0 is the wavelength corresponding to the lowest frequency of operation. This confirms the ultrathin nature of the structure. The absorption performance of the proposed structure has been characterized under normal and oblique incidences followed by their experimental verification. Presented results demonstrate highly polarization-independent behavior of the proposed absorber due to its symmetric geometry. Also, the electromagnetic field distributions have been studied to acquire better insight of the absorption mechanism corresponding to distinct elements present in the structure. It is characterized in terms of its behavior as metamaterial, which ensures the miniaturization. The proposed absorber is suitable to be used in applications like radar cross section reduction, stealth technology, radio frequency identification, and electromagnetic compatibility.

1. Introduction

Metamaterial (MTM) is a division of artificially engineered structures which exhibit simultaneous negative values of permittivity and permeability, therefore enabling researchers to design devices like super lens [1], electromagnetic absorber [2], antenna [3], filter [4], etc. Ever since the investigation by Landy et al. [2] revealed capability of MTM absorbers exhibiting unity absorption, it remains a trending topic among the researchers. MTM absorbers being light weight, compact, and able to realize near unity absorption offer substantial advantages over conventional absorbers.

MTM absorbers (MMAs) have been designed using split ring resonators (SRR) [5], closed ring resonators (CRR) [6], electric-field driven LC resonators (ELC) [7], etc. A typical MMA structure consists of metallic pattern printed over grounded lossy substrate ensuring zero transmission of EM waves through the grounded face. MTM absorbers may be capitalized in terms of their design, size, and ability to be used in wide range of applications. MTM absorbers are also capable of exhibiting wide band [6], single-band [8], dual-band [9, 10], triple-band [11–13], and multiband [14, 15] absorption performances. Wide band absorbers find their applications in stealth technology and anechoic chambers, while multiband absorbers are preferred in applications such as radar cross section reduction, radio frequency identification, sensing, imaging, and various other communication systems. Sometimes, the composite structure of the multiband absorbers provides polarization sensitive absorption attributes [16, 17]. It means their absorption characteristics may get changed due to change in the orientation of the absorber. This is highly undesirable in various practical applications; thus, in the recent years, research focus has been shifted on designing of the multiband polarization insensitive MTM absorber.

Zhai et al. investigated a triple band MTM absorber which comprises a square CRR stacked between two open square rings [11]. Polarization stable behaviour was demonstrated in the paper, and electrical size of the structure was found as 0.119 λ_0 with respect to the lowermost frequency of 3.29 GHz. Later, a triband polarization insensitive absorber using circular fractal structure was proposed by Jiang et al. [12]. This fractal structure consists of circular ring resonators embedded inside an outer circular ring etched over FR4 substrate of 2 mm which negotiate with the electrical size and thickness of the structure. In addition, it offers irregular absorption at the third resonance mode. Furthermore, an MTM absorber using a dual layer approach was suggested, in which each layer of proposed design comprises three star-shaped concentric rings stacked together [13]. It was concluded that the application of dual layer instead of single layer improved absorptivity significantly, but it severely affects the thickness of an MTM absorber along with notable increment in electrical length. Chaurasiya et al. proposed a structure using a circular ring and a mended cross-like structure with curved circular patches placed inside it [14]. Structure being four-fold symmetric is polarization-insensitive, but the unit cell size of the structure is quite large which limits its applications in some practical scenarios. Furthermore, another quad-band MTM absorber consisting of four-solid squares embedded inside an outer square ring is presented for C and X-band applications [15]. This absorber offers polarization insensitivity and wide angle stable absorption along with being ultrathin ($0.0015\lambda_0$). Moreover, a low-profile (0.024 λ_0) penta-band trigeminal-shaped MTM absorber is proposed and investigated in [16], which shows polarization insensitivity at lower frequency and polarization sensitivity at higher frequency in microwave range. Recently, Lakshmi et al. reported a conformal triple band microwave metamaterial absorber, but the rate of absorption is very low at second band [17]. Also, absorption performance is degrading in relation to polarization and incident angle variation due to its complex design. After an intensive literature survey, it is concluded that there are further possibilities of improvement in peak absorptivity along with the miniaturized unit cell size and thickness of the absorber structure. Some of the recent works based on heptaband THz MMAs for biomedical applications and sensing applications are also discussed in [18, 19].

This paper presents a polarization-insensitive and ultrathin quad-band metamaterial absorber for S, C, and Ku band applications. The geometry of the top surface of the investigated structure consists of segmented eight-arm asterick-shaped resonator enclosed by a square ring with trimmed edges. The aforementioned structure is further embedded inside an outer square ring resonator. The proposed structure exhibits absorption characteristics at 3.1 GHz (S-band), 5.42 GHz (C-band), 16.65 GHz (Ku-band), 17.56 GHz (Ku-band), and 20.29 GHz (Ku-band) with absorptivity levels of 99.37%, 99.04%, 98.61%, 95.12%, and 95.57% correspondingly. The full width at half maximum (FWHM) bandwidth is found to be 110 MHz (3.05–3.16 GHz), 200 MHz (5.32–5.52 GHz), 1600 MHz (16.35–17.95 GHz), and 830 MHz (19.87–20.70 GHz) in distinct four bands. Further, surface current and electric field distributions were studied to elaborate the functioning of the proposed structure. The metamaterial property of the suggested MTM absorber is confirmed through effective permeability, permittivity, and dispersion plots. Absorption performance is also studied for transverse electric (TE) and transverse magnetic (TM) polarization for investigating wide incident angle behaviour. The paper is composed as follows: Section 2 elaborates the geometric layout, evolution steps, polarization, and incidence angle stability analysis of the proposed absorber. Electric and magnetic fields are explored to define the absorption phenomenon at different bands which is included in Section 3. The metamaterial behaviour of the proposed unit cell is also explained in this section. Experimental results validating simulated ones and performance comparison of the presented work with specific multiband MTM absorbers are portrayed in Section 3. Section 5 summarizes the features and findings of the suggested work along with futuristic possibilities.

2. Geometry and Progressive Studies of the Suggested Absorber

2.1. Schematic of the Proposed Absorber. Figure 1 displays the schematic layout of the proposed quad-band absorber unit cell with specified design parameters. The structure is constructed on two-sided copper coated (0.035 mm thick) commercial FR4 laminate of permittivity (ε_r) 4.4, dielectric loss tangent (tan δ) 0.02, and thickness 1 mm. The top metallic layer of the intended structure has an inner part as a segmented eight-arm asterick-shaped resonator which is enclosed inside a square ring with trimmed edges at the corners. Furthermore, this ring is encompassed by another square ring which is at the periphery of the unit cell. The absorption rate $A(\omega)$ of the absorber structure is calculated by equation (1) [2].

$$A(\omega) = 1 - \left|S_{11}(\omega)\right|^2 - \left|S_{21}(\omega)\right|^2, \tag{1}$$

where $|S_{11}(\omega)|^2$ and $|S_{21}(\omega)|^2$ refer to the reflected and transmitted powers, respectively. The back side of the designed structure is completely coated with copper; hence, all the incident EM waves will be reflected back and the transmission through absorber structure will be zero, i.e., $|S_{21}(\omega)|^2 = 0$. Therefore, equation (1) can be rewritten as equation.

$$A(\omega) = 1 - \left|S_{11}(\omega)\right|^2 = 1 - \left|\frac{Z_{in}(\omega) - Z_0}{Z_{in}(\omega) + Z_0}\right|^2. \tag{2}$$

The physical dimensions of the unit cell are configured in such a way that the input impedance of the MTM unit cell (Z_{in}) becomes equal to the free space impedance (Z_0) at operating frequency to ensure minimum reflection.

2.2. Evolution Steps of the Proposed Absorber. To know the operation of the absorber, the complete step by step design procedure of the intended absorber is discussed in this section. To illustrate this, proposed structure has been

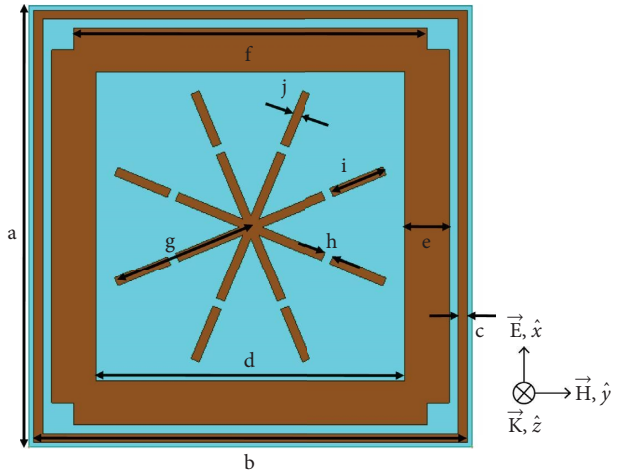

FIGURE 1: Unit cell schematic of the proposed absorber ($a = 10$, $b = 9.8$, $c = 0.2$, $d = 7$, $e = 1$, $f = 8$, $g = 3$, $h = 0.2$, $i = 1.29$, and $j = 0.2$ (All dimensions are in mm)).

analyzed with respect to four distinct configurations that are referred to as Structure-A, Structure-B, Structure-C, and Structure-D as represented in Figure 2. Structure-A implies a square ring, and further on simulation, it gives two absorption bands at 2.93 GHz and 20.78 GHz with peak absorbances of 99.28% and 66.02%, respectively, as seen in Figure 3(a). Moreover, it also offers a spurious band at 15.56 GHz with very less absorptivity of 28.54%. Furthermore, Structure-B shows an inner square ring which has trimmed edges at the corners. Figure 3(a) suggests that it individually offers an absorption band at 4.85 GHz with a significant absorption level of 80.43% and a spurious band at 16.77 GHz with 36.49% absorptivity. An absorption peak is found at 17.13 GHz with absorptivity of 91.49% due to Structure-C, which consists of a segmented 8-arm asterick-shaped resonator. The systematic amalgamation of aforementioned configurations is denoted by Structure-D (proposed structure), and its absorption response is displayed in Figure 3(b). It can be observed that all the bands offered by the individual resonators are intact after combining them with significant improvement in absorptivity. However, this led to right shift of some bands. The proposed structure was excited with the help of Floquet ports, and master-slave boundaries are used as periodic boundaries. The whole simulation of this work was carried out in Ansys Electronics Desktop 2023 R2 Version.

The probable reason for this shift could be the capacitive coupling between the elements. Also, the band due to Structure-C along with spurious bands offered by Structure-A and Structure-B has been merged together, resulting in wide absorption band. Therefore, the suggested absorber exhibits quad-band absorption functionality with peak absorptivity of 99.37%, 99.04%, 98.61%, 95.12%, and 95.57% at 3.1 GHz, 5.42 GHz, 16.65 GHz, 17.56 GHz, and 20.29 GHz, respectively. The full width at half maximum (FWHM) bandwidth is found to be 110 MHz (3.05–3.16 GHz), 200 MHz (5.32–5.52 GHz), 1600 MHz (16.35–17.95 GHz), and 830 MHz (19.87–20.70 GHz).

2.3. Studies of Absorptivity for Different Polarization and Incident Angles. Typically, the performance of microwave absorbers should be intact irrespective of their orientation position and direction of impinging EM wave. In other words, their absorbance characteristics should remain the same with respect to their rotation in azimuthal (xy) plane and change in the incident angles. As suggested in the various literature studies, polarization insensitiveness can be attained using a fourfold symmetric structure. To illustrate the polarization stable characteristics, the proposed absorber is analyzed under different polarization angles (ϕ) varying from 0° to 90° in the xy plane. Figure 4 suggests that the absorptivity level is maintained throughout all the four working bands when polarization angle is varied from 0° to 90°. Therefore, it can be stated that the structure is polarization-insensitive, and hence, it can be placed in any orientation in xy plane.

Next, the absorption behaviour is analyzed with respect to the variation in incident angle under TE and TM polarization as shown in Figures 5(a) and 5(b), respectively. The results assure that the adequate absorptivity is maintained while varying the incident angle from 0° to 45°; however, two additional peaks suddenly emerge near 10 GHz and 12 GHz after incident angle of 45° under both TE and TM polarization cases. The reason for emergence of these spurious bands could be interaction of the incident waves with the different parts of the resonating elements at higher angles. Hence, it is affirmed that the proposed structure indicates appreciable absorption characteristics for a wide range of incidence angles.

3. Parametric Study and Absorption Mechanism of the Proposed Absorber

3.1. Parametric Analysis Study. It is very important to examine the resonance behaviour of the designed absorber with the help of parametric analyses. As it is already discussed in the previous section that the first band is originated due to outer square ring only; therefore, in this section, we have considered the design variables that are responsible for exciting bands other than the first band. We altered the two parameters, namely, the width of inner square ring having trimmed edges (e) and the gap between the fragments of segmented asterick-shaped resonators (h) and studied its effect on the absorptivity performance of the entire structure. All the simulation work carried out in this paper is as follows.

3.1.1. Variation in Width (e) of Ring with Trimmed Edges. In this analysis, e has been varied from 0.6 mm to 1.4 mm as shown in Figure 6. When e is increased, the fourth band gets shifted towards lower frequency due to increase in coupling capacitance between outer and inner rings. In addition, its effect is less pronounced on first two bands. However, the third band is shifting randomly due to the combined effect of change in the gaps among the segmented asterick-shaped resonator and inner and outer rings. A good absorption rate and bandwidth are achieved at $e = 1$ mm.

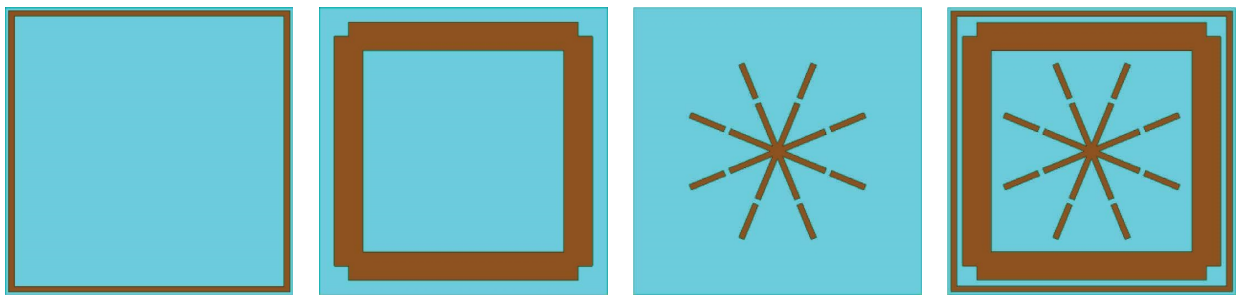

Figure 2: Evolution of the proposed absorber by means of different configurations: (a) Structure-A, (b) Structure-B, (c) Structure-C, and (d) Structure-D.

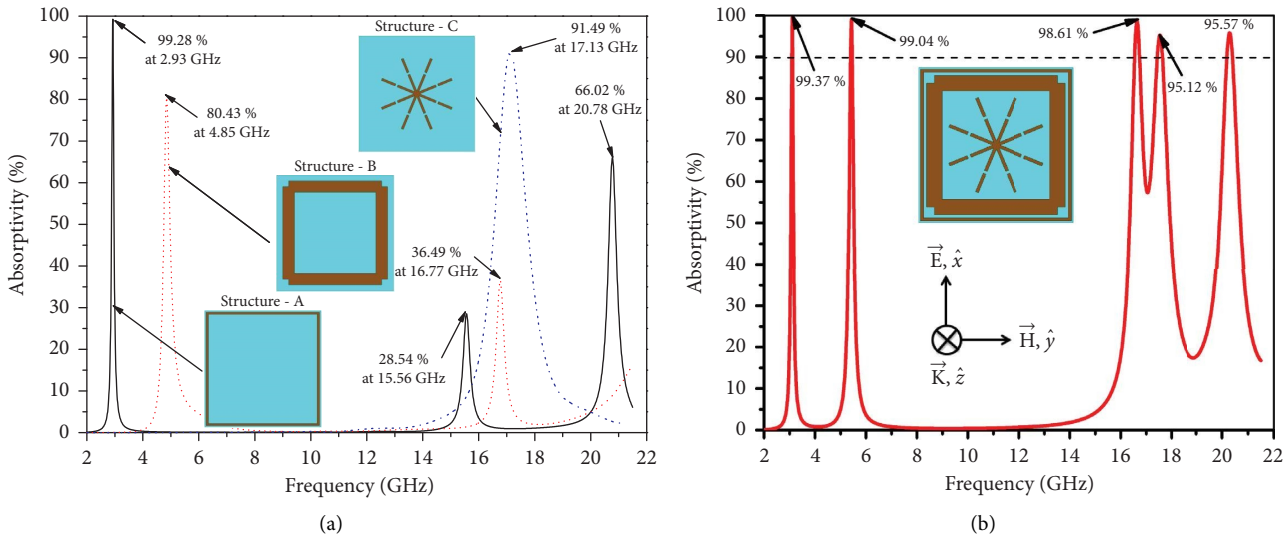

Figure 3: Simulated absorptivity of (a) different configurations of the designed absorber and (b) the proposed absorber.

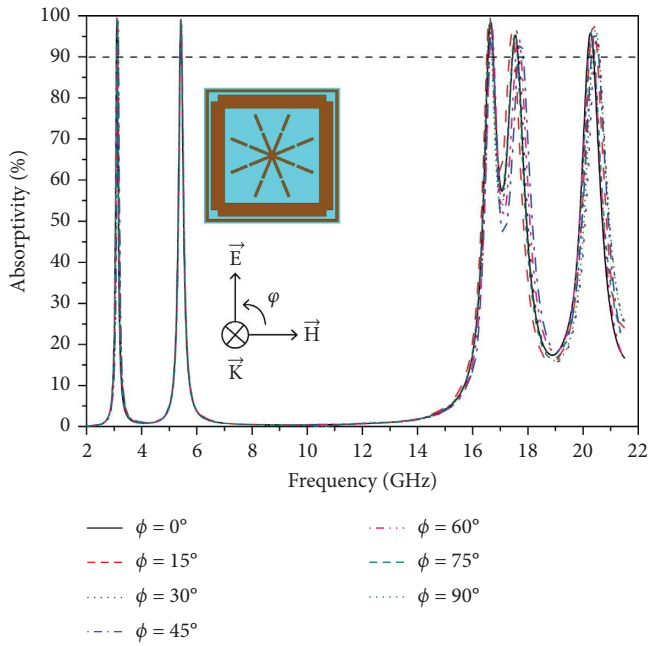

Figure 4: Simulated absorptivity of the proposed absorber for different azimuthal angles (ϕ).

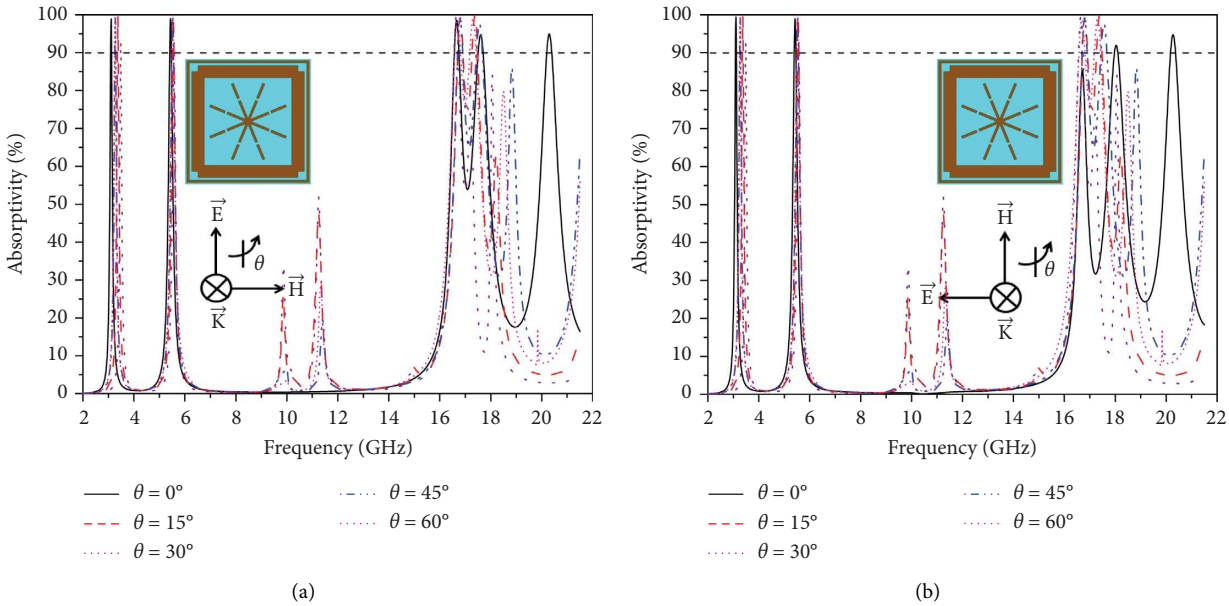

Figure 5: Simulated absorption curves considering various incident angles under (a) TE polarization and (b) TM polarization.

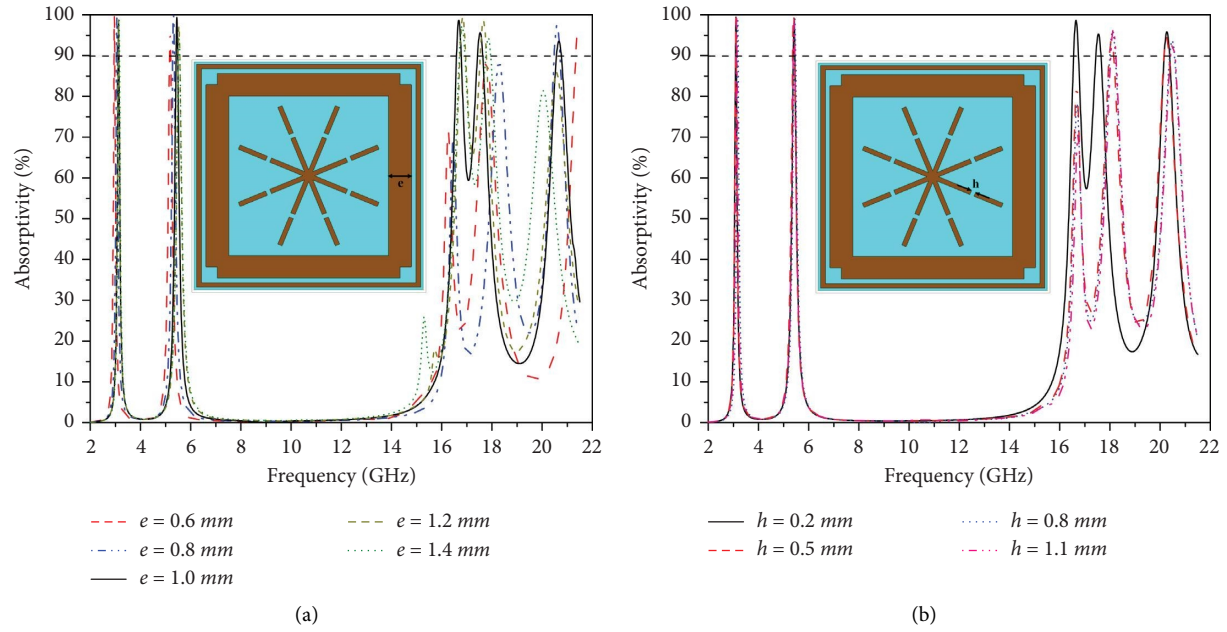

Figure 6: Effect on the absorption coefficient of the proposed absorber on varying (a) e and (b) h.

3.1.2. Variation in the Gap of Segmented Star Shape (h). Parameter h is also an important design parameter as it is used to tune the higher absorption bands. To verify the same, h is varied from 0.2 to 1.1 mm. Note that first two bands and fourth band are contributed by outer and inner rings only; hence, no effect of this variation is observed on first two bands, while there is a negligible effect on the fourth band. As h increases, third absorption band is decreased gradually as this band arises due to the fragmented structure. A good absorption rate and bandwidth are obtained at $h = 0.2$ mm.

3.2. Electric Field and Surface Current Distribution Study. Electric field and surface current distribution analyses are utmost useful to get better insight of absorption mechanism. Literature studies suggest that high electric field concentration is related to the electric excitation and the magnetic resonance can be represented by circulatory flow of surface current.

Figure 7 displays the electric field distribution at all the five absorption peak frequencies. After analyzing the electric field distributions in Figures 7(a) and 7(e), it is found that

there is strong electric field concentration present in the outer ring resonator at 3.10 GHz and 20.29 GHz. It means that the first and last absorption bands are solely due to outer square ring. It is seen from Figure 7(b) that, at 5.42 GHz, a notable amount of electric field is populated in horizontal limbs of the inner trimmed ring resonator and outer square ring. It is stated in sub-Section 2.2 that the second band is originated due to square ring with trimmed edges, but it got shifted to the higher frequency due to capacitive coupling between outer and intermediate rings. So, outer and inner rings play a pivotal role in introduction of absorption band at 5.42 GHz. The study of field distribution at 16.65 GHz and 17.56 GHz as depicted in Figures 7(c) and 7(d), respectively, reveals that the segmented asterick-shaped resonator plays a vital role in origination of third band as its inner edges experience the highest electric field intensity. A little amount of electric field can also be noticed on the edges of the inner trimmed ring resonator and some parts of the outer ring.

Figure 8 depicts the surface current distribution at all the frequencies where the proposed structure exhibits maximum absorption. A careful study of surface current distribution demonstrates that it is following the same pattern as electric field. In addition, the surface current on front and rear faces is in antiparallel direction at all the frequencies, which gives rise to magnetic excitation. The above study corroborates the statements made in sub-Section 2.2 about the contribution of various parts in absorption and provides better understanding of the absorption process of the proposed structure.

3.3. Analysis of the Proposed Unit Cell for MTM Characteristics. Recent research reports recommend that employing MTM is one of the best techniques to achieve miniaturization of microwave structures. Therefore, the proposed unit cell has been characterized to examine the metamaterial behaviour. To do this, firstly, two-port analysis was performed on the proposed unit cell applying master-slave boundary conditions and Floquet port excitation. Subsequently, permittivity and permeability characteristics have been retrieved with the help of the MATLAB script [20] using the S parameter extraction method of the unit cell described in [21]. Figures 9(a) and 9(b) show the curve of the real and imaginary parts of the permittivity and permeability, respectively.

The values of permittivity and permeability at peak absorption frequencies obtained from Figure 9 are noted in Table 1 for better grasp. It can be noticed that the real part of permittivity and permeability at 17.56 GHz are negative, thus confirming the metamaterial property of the proposed absorber. Also, at other frequencies except for 16.65 GHz, the real part of permeability is negative and permittivity is close to negative. These retrieved parameters are quite close to each other which satisfy the condition of maximum absorption. The values being very close implies that the input impedance of the medium matches perfectly with the free space impedance. This leads to minimal reflections and maximum absorptivity.

Left-handed property of the metamaterials can be explained with the help of the dispersion diagram. To demonstrate this characteristic, dispersion profile of the proposed structure is plotted in Figure 10. Any dispersion curve can be classified into two regions, right-handed (RH) region and left-handed (LH) region. LH region indicates the area where the plot has a negative slope while the RH region has a positive slope. This curve has been obtained with the help of equation (3) [21]:

$$\beta d = \cos^{-1}\left(\frac{1 - S_{11}S_{22} + S_{12}S_{21}}{2S_{21}}\right), \tag{3}$$

where d represents the periodicity of the unit cells. Figure 10 demonstrates that the first band lies in the LH region, whereas the other three bands lie in the composite right/left-handed (CRLH) region. Hence, the proposed structure can be regarded as the MTM-based structure and thus achieves miniaturization.

4. Experimental Results and Validation

The proposed absorber is implemented on a 1 mm thick and 1Feet^2 FR4 laminate to validate the absorbance behaviour as shown in Figure 11. The experiments were conducted in a free space environment using the method outlined in [21, 22]. The measurement was carried out using Anritsu S820E (1 MHz–30 GHz) handheld vector network analyzer (VNA) and two standard horn antennas covering the entire range of the operation. VNA was calibrated over the range of 2 GHz–22 GHz before performing the measurements. Initially, reflection from a copper sheet of the identical size was recorded to take the losses due to free space into consideration. Later on, the absorber prototype was placed at exactly the same position to obtain the reflections from it. The difference between the later and former provides the reflection coefficients of the proposed absorber. Finally, absorptivity can be easily calculated with the help of the relation expressed in equation (2). Figure 12 provides measured absorptivity in comparison with the simulated one. It can be seen that experimental results follow well with those of the simulated ones. Experimental results show that fabricated prototype exhibits all the four bands perfectly. The measured FWHM bandwidth is noted to be 250 MHz (3.01–3.26 GHz), 310 MHz (5.24–5.55 GHz), 1640 MHz (16.20–17.84 GHz), and 940 MHz (19.91–20.85 GHz). The peak absorptivity of 99.29%, 98.59%, 97.32%, 98.62%, and 96.29% is achieved at 3.17 GHz, 5.42 GHz, 16.58 GHz, 17.57 GHz, and 20.54 GHz, respectively. Minor shift in the upper band is observed which may be due to the fabrication tolerance in gap of the segmented arm. Furthermore, significant distortions could be monitored in nonabsorption regions which are the adverse effects of performing measurement in free space instead of anechoic chamber. Essentially, the unwanted radiations from the surrounding bodies received by the horn antennas cause these hindrances in the measured absorptivity results.

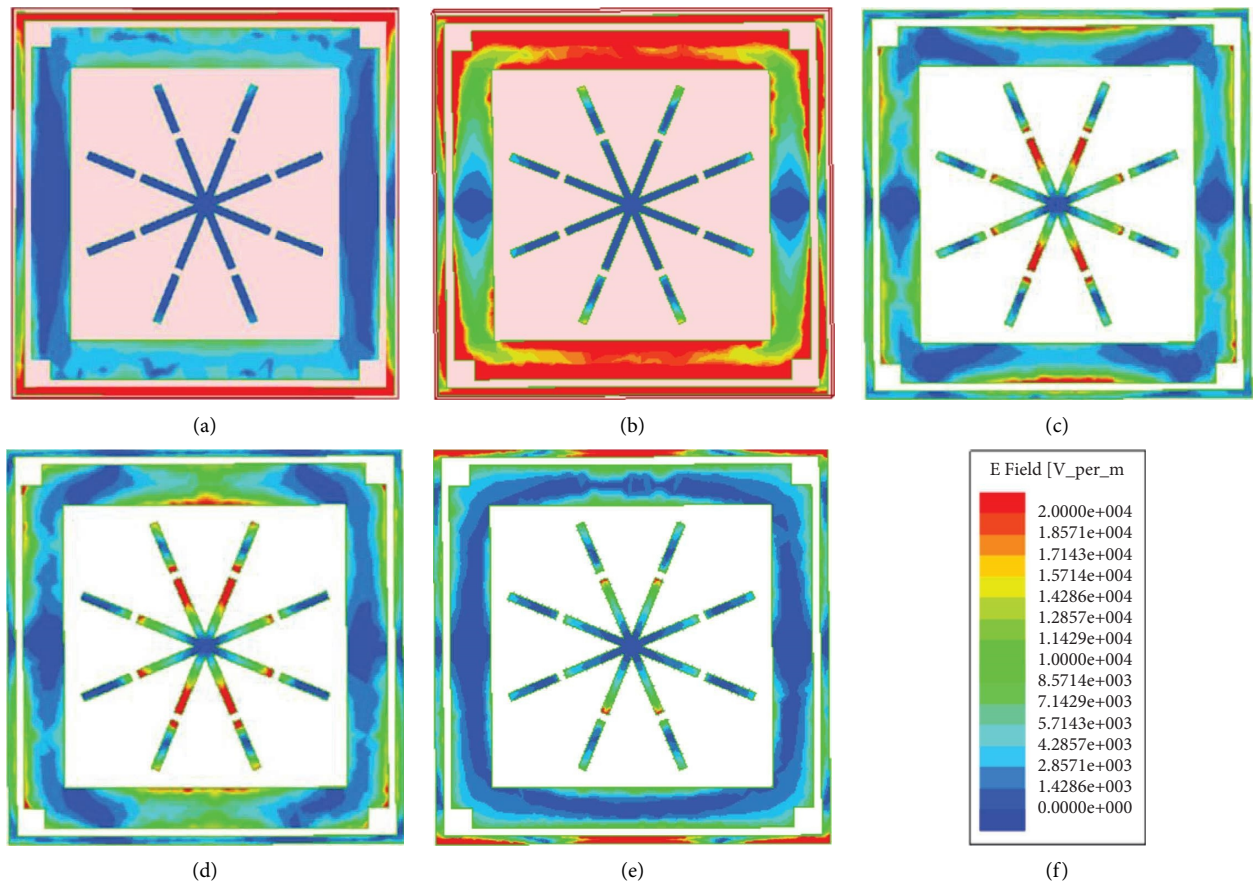

Figure 7: Electric-field distribution of the proposed absorber at (a) 3.10 GHz, (b) 5.42 GHz, (c) 16.65 GHz, (d) 17.56 GHz, (e) 20.29 GHz, and (f) magnitude scale.

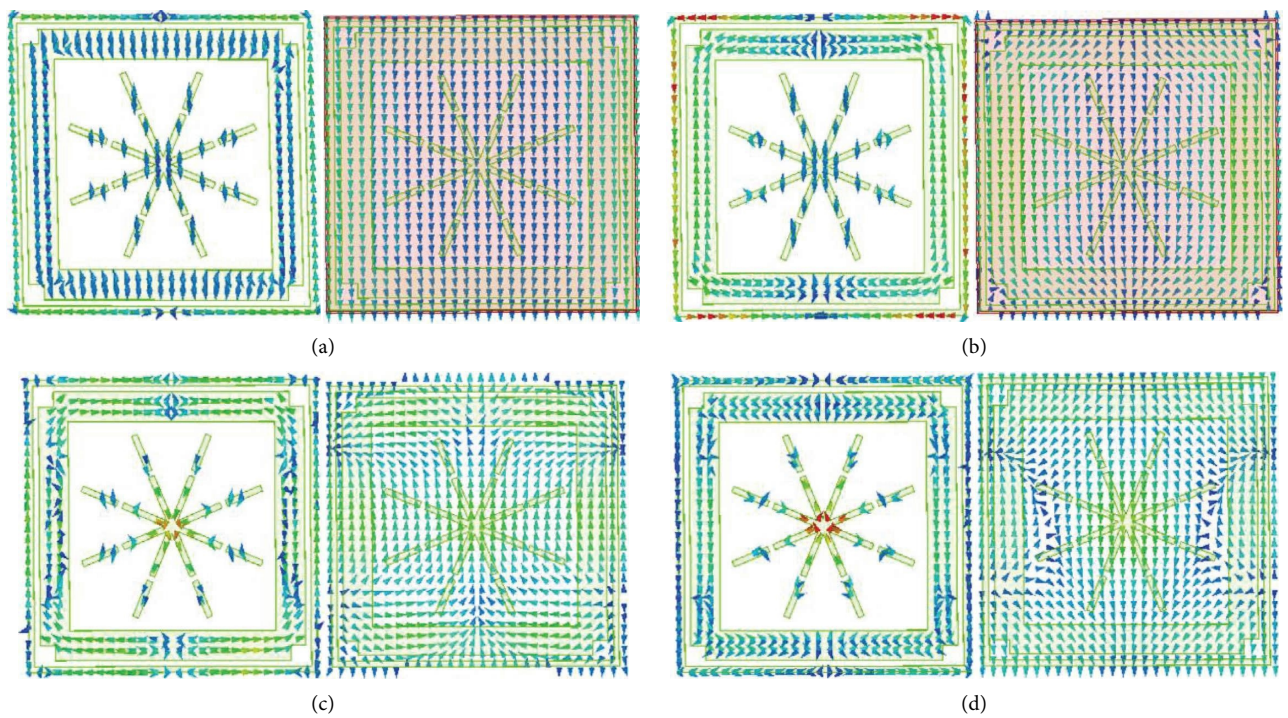

Figure 8: Continued.

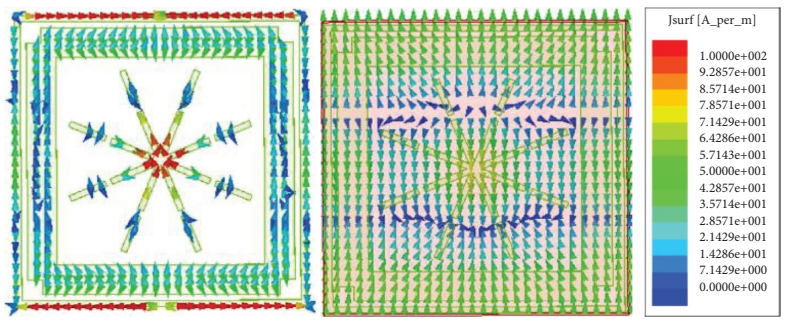

(e)

Figure 8: Surface current at the top and bottom faces of the proposed structure at (a) 3.10 GHz, (b) 5.42 GHz, (c) 16.65 GHz, (d) 17.56 GHz, and (e) 20.29 GHz.

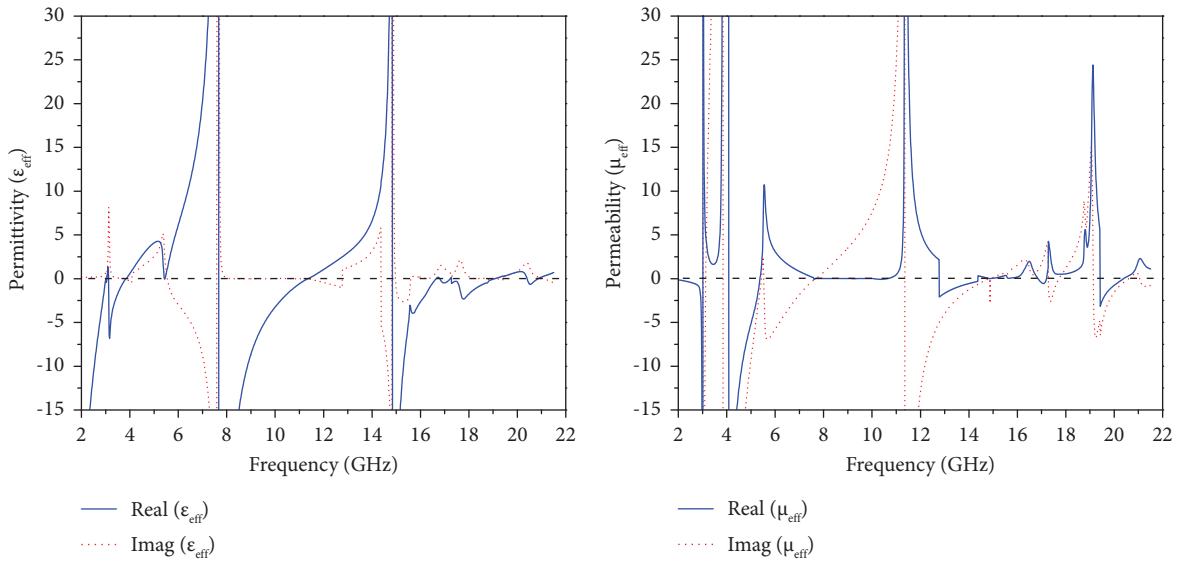

(a) (b)

Figure 9: Extracted material parameters of the proposed unit cell: (a) permittivity and (b) permeability.

Table 1: Effective material parameters obtained at peak absorption frequencies.

Abs. freq. (GHz)	Permittivity (ε_{eff})		Permeability (μ_{eff})	
	Real	Imaginary	Real	Imaginary
3.1	1.34	3.48	−10.67	6.77
5.42	0.05	3.54	−0.39	0.99
16.65	0.009	0.69	0.46	0.98
17.56	−0.55	1.78	−0.97	0.59
20.29	0.66	1.55	−0.68	0.20

Abs. freq. = Absorption frequency.

After this, polarization free behaviour of the proposed absorber is confirmed experimentally. To do this, the fabricated prototype is rotated in the xy plane while keeping the position of the horn antennas fixed. First, a copper sheet of identical size was placed at different angles from 0° to 90° in the step size of 15°, and corresponding reflections received at the horn antenna were recorded. The same procedure is then followed for the prototype, and the reflections at the receiver horn antenna were stored. The difference between both the cases provides the reflection coefficients for varying azimuthal angles (ϕ). Equivalent absorptivity is then calculated and is plotted in Figure 13(a). It can be deduced that the proposed absorber is functioning well without any deviation in the absorptivity level. It is a very important characteristic which enables users to position the absorber orientation whichever way it is needed in the xy plane. Figure 13(b)

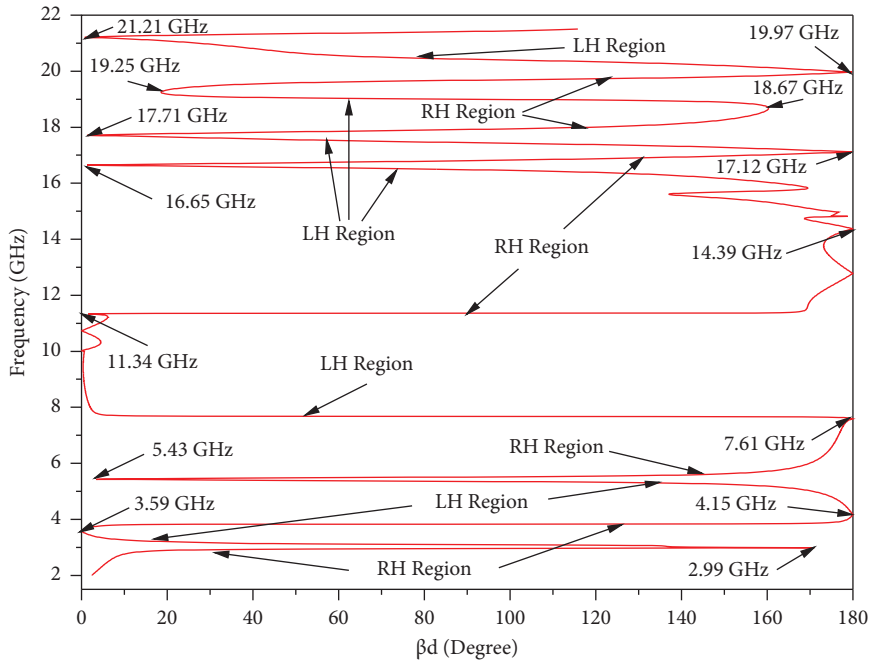

Figure 10: Dispersion characteristics of the proposed absorber.

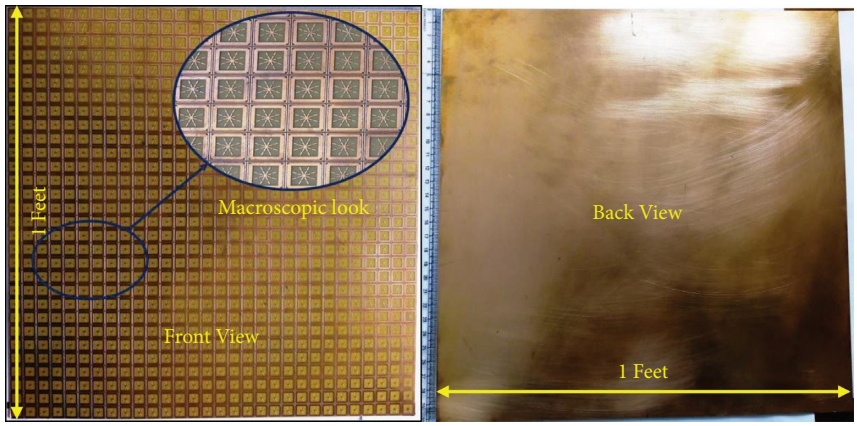

Figure 11: Snapshots of the fabricated prototype sheet adopted for the experimental results.

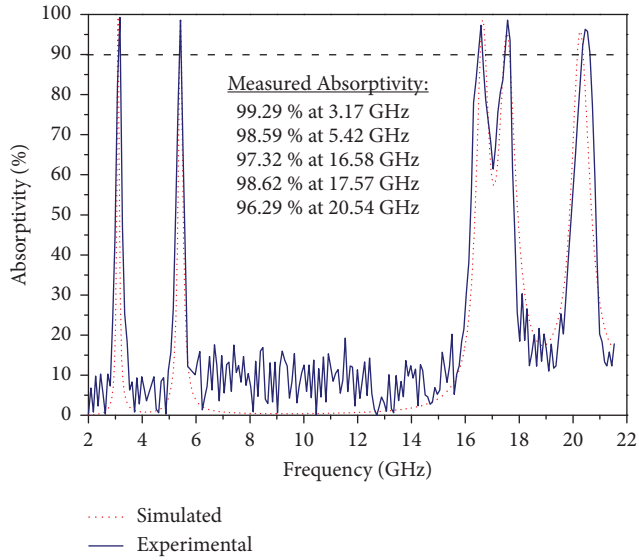

Figure 12: Simulated and experimental absorptivity of the proposed absorber.

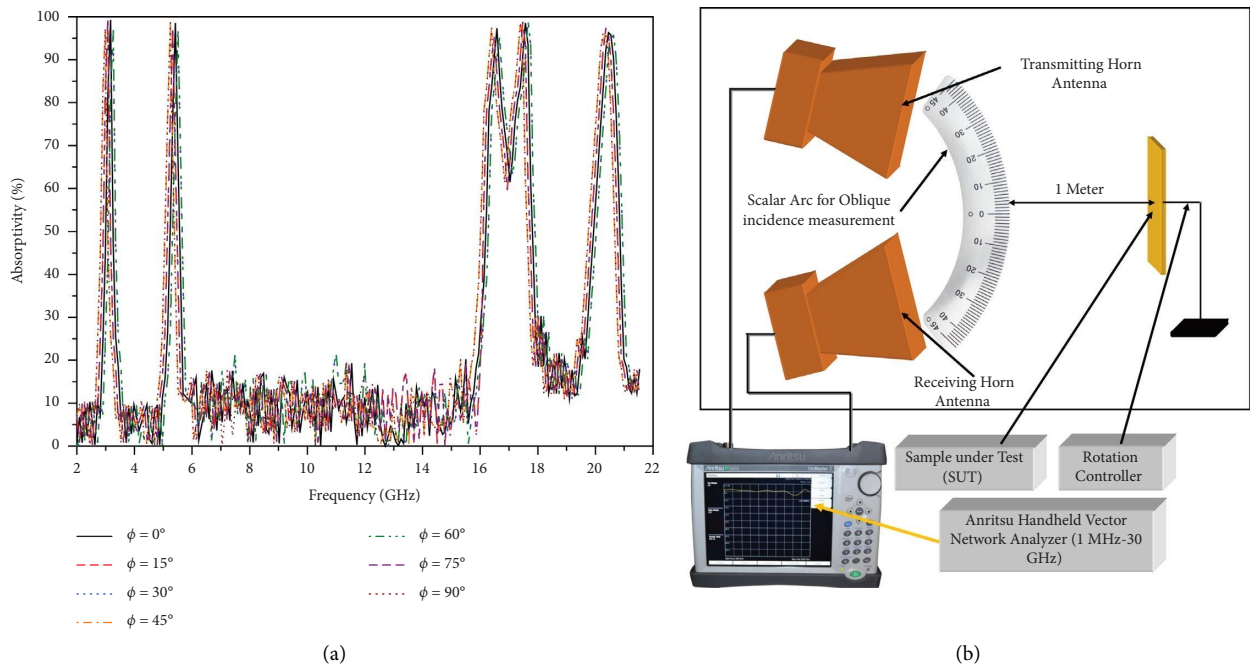

FIGURE 13: (a) Measured absorptivity of the proposed absorber under normal incidence by varying azimuthal angle (ϕ) and (b) experimental setup created for measuring the absorptivity responses for normal and oblique incidences.

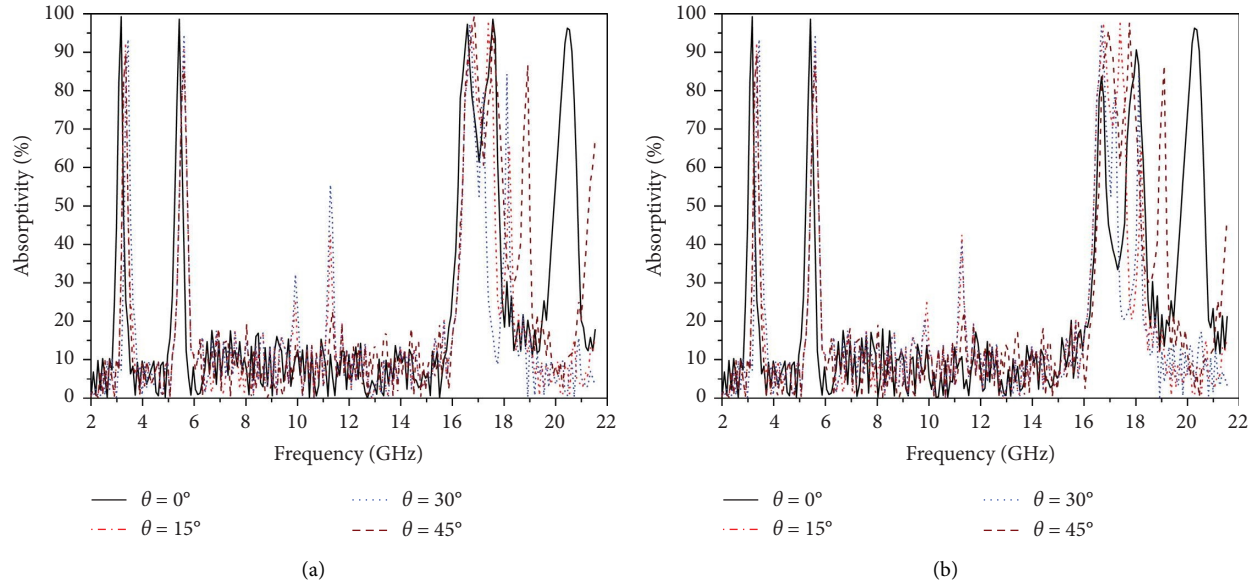

FIGURE 14: Absorptivity of the proposed absorber for varying incident angles (θ) under (a) TE polarization and (b) TM polarization.

displays the experimental setup for carrying out the absorptivity measurements under normal and oblique incidences in free space. Next, the proposed absorber was also characterized under oblique incidence variations, and an arrangement was established provisionally. Under this setup, an arc was drawn on the floor to adjust the positions of the horn antennas (as per Snell's law of reflection) at different angles from 0° to 45° in the step size of 15° while keeping the absorber sample under test fixed. Figures 14(a) and 14(b) illustrate the results obtained from the oblique incidence measurements under TE and TM polarization cases, respectively. Spurious bands near 10 GHz and 12 GHz are emerged at 30° and 45° as noted in the simulated results. All bands are intact when EM waves are incident obliquely on the surface of the absorber. Thus, it can be said that the proposed absorber is suitable for wide incident angle absorption.

The proposed work is compared particularly with the recently reported metamaterial-based ultrathin multiband absorbers, and summary is presented in Table 2. In the table,

Table 2: Comparison of the proposed work with recently reported MTM-based absorbers.

(References)	Lowest absorption frequency (LAF) (GHz)	Unit cell size (mm^2)	Unit-cell size with respect to LAF (λ_0)	Thickness with respect to LAF (λ_0)	Number of bands	Polarization independent
[11]	3.25	11×11	0.119	0.0112	3	Yes
[12]	2.29	30×30	0.229	0.015	3	Yes
[13]	1.8	34.8×34.8	0.209	0.0294	3	Yes
[14]	4.11	15×15	0.205	0.013	4	Yes
[15]	4.34	20×20	0.289	0.011	4	Yes
[16]	5.984	17×17	0.339	0.024	5	No
[17]	11.4	10×10	0.380	0.0038	3	No
[23]	2.24	20×20	0.149	0.0112	4	Yes
This work	3.1	10×10	0.103	0.0103	4	Yes

λ_0 represents the free-space wavelength which corresponds to the lowest absorption frequency (LAF). It illustrates that the proposed absorber is miniaturized in nature as compared to all other MTM-based absorbers. Also, it offers polarization-insensitive behaviour with four numbers of bands. Moreover, the thickness of the intended absorber is smaller than that of the compared works; thus, it can be said that the suggested absorber can be employed for radar cross section reduction, stealth technology, radio frequency identification, and electromagnetic compatibility applications in the S, C, and Ku bands.

5. Conclusion

A novel, miniaturized, ultrathin, and polarization insensitive metamaterial inspired quad-band absorber has been studied and realized in this paper. Polarization free and wide incidence angle stable properties of the suggested absorber have been confirmed with the help of absorption performance under normal and oblique incidences, respectively, which was also validated through subsequent measurements. The study of electric field and surface current distribution authenticates the inferences drawn during parametric investigations. Moreover, the metamaterial property of the proposed structure was also elaborated using permittivity, permeability, and dispersion plots. Compared to other reported MTM-based microwave absorbers, the proposed structure offers much better electrical thickness of 0.0103 λ_0 except for the absorber reported in [17]. The proposed work suggests further opportunities in enhancing the miniaturization and ultrathin nature of the microwave absorbers exhibiting multiple bands.

Data Availability

The data used to support the findings of this study are included within the article.

Disclosure

A preprint of this work is available in [24].

Conflicts of Interest

The authors declare that there are no conflicts of interest regarding the publication of this paper.

References

[1] N. Fang, H. Lee, C. Sun, and X. Zhang, "Sub diffraction-limited optical imaging with a silver super lens," *Science*, vol. 308, no. 5721, pp. 534–537, 2005.

[2] N. I. Landy, S. Sajuyigbe, J. J. Mock, D. R. Smith, and W. J. Padilla, "Perfect metamaterial absorber," *Physical Review Letters*, vol. 100, no. 20, Article ID 207402, 2008.

[3] R. K. Singh and A. Gupta, "An asymmetric CPW-fed ultra miniaturized epsilon negative triple band antenna with improved gain using complimentary closed ring resonators," *Journal of Electromagnetic Waves and Applications*, vol. 36, no. 17, pp. 2582–2599, 2022.

[4] R. K. Singh and A. Gupta, "A miniaturized highly selective MTM-inspired filter for low-pass and triple-band band-pass performance with configurable transmission zeros and bandwidth," *International Journal of Circuit Theory and Applications*, vol. 51, no. 8, pp. 3695–3709, 2023.

[5] M. Bağmancı, O. Akgöl, M. Özaktürk, M. Karaaslan, E. Ünal, and M. Bakır, "Polarization independent broadband metamaterial absorber for microwave applications," *International Journal of RF and Microwave Computer-Aided Engineering*, vol. 29, no. 1, Article ID 21630, 2019.

[6] S. Ghosh, S. Bhattacharyya, D. Chaurasiya, and K. V. Srivastava, "An Ultra-wideband ultra-thin metamaterial absorber based on circular split rings," *IEEE Antennas and Wireless Propagation Letters*, vol. 14, pp. 1172–1175, 2015.

[7] D. Sood and C. Tripathi, "Quad band electric field-driven LC resonator-based polarisation-insensitive metamaterial absorber," *IET Microwaves, Antennas & Propagation*, vol. 12, no. 4, pp. 588–594, 2018.

[8] B. Wang, T. Koschny, and C. M. Soukoulis, "Wide-angle and polarization-independent chiral metamaterial absorber," *Physical Review B*, vol. 80, no. 3, Article ID 33108, 2009.

[9] S. Bhattacharyya, S. Ghosh, and K. V. Srivastava, "A dual band metamaterial absorber using electric field driven LC (ELC) and cave ELC structures," in *Proceedings of the 2013 IEEE Antennas and Propagation Society International Symposium (APS URSI)*, pp. 1452-1453, Orlando, FL, USA, July 2013.

[10] D. Chaurasiya, S. Ghosh, S. Bhattacharyya, and K. V. Srivastava, "Dual-band polarization-insensitive metamaterial absorber with bandwidth-enhancement at Ku-band for EMI/EMC application," in *Proceedings of the 2014 IEEE International Microwave and RF Conference (IMaRC)*, pp. 96–99, Bangalore, India, December 2014.

[11] H. Zhai, C. Zhan, Z. Li, and C. Liang, "A Triple-band ultrathin metamaterial absorber with wide-angle and polarization

stability," *IEEE Antennas and Wireless Propagation Letters*, vol. 14, pp. 241–244, 2015.

[12] H. Jiang, Z. Xue, W. Li, and W. Ren, "Multiband polarisation insensitive metamaterial absorber based on circular fractal structure," *IET Microwaves, Antennas & Propagation*, vol. 10, no. 11, pp. 1141–1145, 2016.

[13] K. P. Kaur and T. Upadhyaya, "Wide-angle and polarisation-independent tri-band dual-layer microwave metamaterial absorber," *IET Microwaves, Antennas & Propagation*, vol. 12, no. 8, pp. 1428–1434, 2018.

[14] D. Chaurasiya, S. Ghosh, S. Bhattacharyya, A. Bhattacharya, and K. V. Srivastava, "Compact multi-band polarisation-insensitive metamaterial absorber," *IET Microwaves, Antennas & Propagation*, vol. 10, no. 1, pp. 94–101, 2016.

[15] M. Agarwal, A. K. Behera, and M. K. Meshram, "Wide-angle quad-band polarisation-insensitive metamaterial absorber," *Electronics Letters*, vol. 52, no. 5, pp. 340–342, 2016.

[16] H. Wu, S. Ji, J. Zhao, C. Jiang, and H. Dai, "Design and analysis of a five-band polarization-insensitive metamaterial absorber," *International Journal of Antennas and Propagation*, vol. 2020, Article ID 8827517, 12 pages, 2020.

[17] M. L. S. N. S. Lakshmi, S. P. J. Christydass, S. Kannadhasan, K. Anguraj, and J. M. Chatterjee, "An efficient triband metamaterial absorber is presented for X- and K-band applications," *International Journal of Antennas and Propagation*, vol. 2023, Article ID 6065300, 9 pages, 2023.

[18] P. Jain, H. Chhabra, U. Chauhan et al., "Machine learning assisted hepta band THz metamaterial absorber for biomedical applications," *Scientific Reports*, vol. 13, no. 1, p. 1792, 2023.

[19] P. Jain, K. Prakash, N. Sardana, K. Sanjeev, G. Neena, and K. S. Arun, "Design of an ultra-thin hepta-band metamaterial absorber for sensing applications," *Optical and Quantum Electronics*, vol. 54, no. 9, p. 569, 2022.

[20] A. B. Numan and M. S. Sharawi, "Extraction of material parameters for metamaterials using a full-wave simulator [education column]," *IEEE Antennas and Propagation Magazine*, vol. 55, no. 5, pp. 202–211, 2013.

[21] R. K. Singh and A. Gupta, "A wrenched-square shaped polarization independent and wide angle stable ultra-thin metamaterial absorber for S-band, X-band and Ku-band applications," *AEU-International Journal of Electronics and Communications*, vol. 132, Article ID 153648, 2021.

[22] S. Bhattacharyya, S. Ghosh, and K. Vaibhav Srivastava, "Triple band polarization-independent metamaterial absorber with bandwidth enhancement at X-band," *Journal of Applied Physics*, vol. 114, no. 9, Article ID 94514, 2013.

[23] M. Edries, H. A. Mohamed, S. S. Hekal, M. A. El-Morsy, and H. A. Mansour, "A new compact quad-band metamaterial absorber using interlaced I/square resonators: design, fabrication, and characterization," *IEEE Access*, vol. 8, pp. 143723–143733, 2020.

[24] R. K. Singh, A. Gupta, A. Yadav, N. Gupta, and U. Tyagi, "A low profile asterick-shaped polarization free metamaterial-inspired absorber for penta-band characteristics," 2021, https://europepmc.org/article/ppr/ppr377530.